PCCP

Accepted Manuscript

ROYAL SOCIETY OF CHEMISTRY

www.rsc.org/pccp

Band Gap Engineering of FeS_2 under Biaxial Strain: A First Principles Study

Pin Xiao,[1,2] Xiao-Li Fan,[1,2] Li-Min Liu[2,3] and Woon-Ming Lau[2,3]*

[1] School of Material Science and Engineering, State Key Laboratory of Solidification Processing, Northwestern Polytechnic University, 127 YouYi Western Road, Xi'an, Shaanxi 710072, China

[2] Beijing Computational Science Research Center, Beijing 100084, China

[3] Chengdu Green Energy and Green Manufacturing Technology R&D Center, Chengdu, Sichuan 610207, China

[*] xlfan@nwpu.edu.cn [*] limin.liu@csrc.ac.cn

Abstract

Promising photovoltaic activity from pyrite (FeS_2) is attributed to its excellent optical absorptivity and earth abundance, but its band gap, 0.95 eV, is slightly lower than the optimum value of 1.3 eV. Here we report a first investigation of strained FeS_2, whose band gap can be increased by ~0.3 eV. The influence of uniaxial and biaxial strain on atomic structure, as well as electronic and optical properties of bulk FeS_2 are systematically examined by the first principles calculation. We found that the biaxial strain can effectively increase the band gap with respect to uniaxial stain. Our results indicate that the band gap increases with increasing tensile strain to its maximum value at 6% strain, but under the increasing compressive strain, the band gap decreases almost linearly. Moreover, the low intensity conduction states near Fermi level disappear and the sharp rise starts at the lower energy level under the tensile strain, which causes the red shift of the absorption edge and enhances the overall optical absorption. With the enlargement of band gap and enhanced optical absorption,

FeS_2 will make better photovoltaic materials.

Keywords: FeS_2, biaxial strain, band structure, optical adsorption, density functional theory

I. Introduction

Pyrite (FeS_2) has received intense attention as promising photovoltaic material because of its high abundance, nontoxicity, and strong light absorption (~10^5 cm^{-1} for hν > 1.4 eV).[1, 2] The monocrystalline FeS_2 photoelectrodes and solid-state Schottky solar cells of FeS_2 have shown large short-circuit current densities (30−42 mA/cm^2) and quantum efficiencies (up to 90%).[3, 4] However, energy conversion efficiency of pyrite solar cells is still limited by its low open-circuit voltage (OCV) which is less than 0.2 eV.[3] Various possible explanations have been proposed for the low OCV, including bulk defects,[5-8] intrinsic surface states,[8-11] the low intensity states at the bottom of the conduction band,[12] and the presence of competing phases (most notably marcasite).[9] Most importantly, according to Shockley-Queisser theory,[13] optimum band gap of FeS_2 is 1.3 eV, which is defined as the band gap value of semiconductors at which the theoretical energy conversion efficiency get 31% in the single-junction photovoltaic application. However, the band gap of FeS_2 is 0.95 eV, which is far narrow for optimal photovoltaic applications although it is small enough for FeS_2 to absorb a wide range of solar spectrum. In order to develop the pyrite-based photovoltaics, modulating band gap of FeS_2 is greatly necessary to mediate the long-standing problem of its low OCV.

In semiconductor production, doping is one of the most feasible methods to modulate its electronic properties. In this context, alloyed FeS_2 with either suitable anions (such as O, As, *etc.*) or

cations (such as Ru, Os, Zn, *etc.*) has been widely studied.[6, 14-19] Based on the theoretically studies by Sun *et al* [6] and Hu *et al*, [15] the band gap of FeS_2 can be increased by anion alloying with oxygen. However, incorporating oxygen into FeS_2 is not easy to control because oxygen may react with Fe component.[2] On the other hand, although density functional theory calculations predicted that Ru or Os alloying increases the band gap of FeS_2 by about ~0.1 eV at 50% incorporation concentrations, the incorporation is very limited due to the low solubility of Ru and Os in FeS_2, and the elements Ru and Os are not naturally abundant.[16] Additional, the earth abundant and low cost Zn alloying makes the band-gap of FeS_2 narrow down significantly at 50% incorporation concentrations,[15, 16] and the application of alloyed FeS_2 films with Sn, Mn is very limited due to its high cost although experiment has shown that its band gap has been increased.[17-19] Thus, an effective approach to increase the band gap of pyrite is still under discussion.

Besides introducing impurities, the band structure of semiconductor could also be modified by the interatomic distances and relative atomic position.[20-24] Hence, external pressure may alter the electronic structure of semiconductors. Previous theoretical studies have predicted that the band gap of bulk FeS_2 increases under negative pressure.[20, 22] Eyert *et al.*[20] have demonstrated that the band gap of FeS_2 increases by 0.37 eV after moving the sulfur atoms by less than 1% of the lattice constant. They also concluded that the upshift of the conduction band minimum results from the decrease of sulfur-sulfur bonds, which decreases the band dispersion at the conduction band minimum. But Muscat *et al.* [22] have demonstrated that the increase of sulfur-sulfur bonds make the conduction band minimum move up and the band gap increase by ~0.2 eV at -15 GPa. The decrease of band gap was also demonstrated by theoretical and experimental studies under positive pressure.[20-22, 25, 26] Besides pressure, the strain also may be used to modify the band structure. Recent

theoretical studies[27-29] have predicted that the band gap of Ge is converted from indirect to direct under uniaxial tensile strain, and the value of band gaps of both Si and Ge decrease under uniaxial and biaxial compressive strain.

As we all know that the application of pressure is important in three dimension semiconductors, while strain is more applicable in two dimension semiconductors. In photovoltaic applications, the epitaxial growth of FeS_2 thin film proceeds with orientation [100] on the substrate.[18, 19, 30, 31] Consequently, biaxial strain may be introduced on the FeS_2 thin films, and the band gap of FeS_2 may be adjusted. However, to our knowledge, the investigations on the physical properties of strained FeS_2 is still lacking. In the present work, we carried out first-principles calculations on the atomic structure, electronic and optical properties of FeS_2 under compressive and tensile strain ranging from 0% to 12%. The band gap of FeS_2 subjected to both uniaxial and biaxial strain were investigated.

II. Computational methods

All the calculations in the present study were performed by adopting the spin-polarized density functional theory (DFT), as implemented in the Vienna ab initio simulation package (VASP) code.[32] The ion-electron and electron-electron interactions were calculated by the projector augmented plane-wave (PAW) method,[33, 34] and a plane-wave basis set. The generalized gradient approximation (GGA) of the Perdew-Burke-Ernzerhof formula[35] plus Hubbard U approach[36] (PBE+U) was used to calculate the electronic exchange-correlation potential. We used an effective U of 2 eV, which had been shown to give a good description of bulk properties of FeS_2.[5] Based on the Monkhorst−Pack scheme,[37] Brillouin zone integration was carried out at 7 × 7 × 7 k-mesh, and 11 × 11 × 11 k-mesh were used to calculate the density of states (DOS). A cutoff 400 eV was selected for the plane wave

basis set. The convergence criterion for energy was set as 1×10^{-5} eV. All the atoms were fully relaxed until the force on each atom was smaller than 0.01 eV/Å. The charge populations were calculated using Bader's atom in molecule (AIM) method based on charge density topological analysis.[38] The charge density in real space is reconstructed properly from the PAW method,[39] an intensive grid of 72 x 72 x 72 was adopted to reproduce the total core charge accurately.

Biaxial strain were imposed in the (100) plane of FeS_2, the term "in-plane" refers to the (100) plane, and "out-of-plane" means the direction perpendicular to the (100) plane, which is the [100] direction. To model FeS_2 under certain biaxial strain, the in-plane lattice constant a was fixed at a specific value a_0, and the out-of-plane lattice constant a was relaxed during the structural optimization. The in-plane and out-of-plane strain are related to lattice constant through

$$\eta_{//} = \eta_{010} = \eta_{001} = (a_0 - a) / a \qquad (1)$$

and

$$\eta_{\perp} = (\alpha_r - \alpha) / a \qquad (2)$$

respectively. η_{010} and η_{001} represent the strain along [010] and [001] directions in (100) plane. a_r is out-of-plane lattice constant after relaxation under the biaxial strain . The uniaxial strain is imposed along [001] direction through fixing the lattice constant along [001] direction and relaxing those along the other two directions, and the lattice constant are set via formula (1). In the present study, $\eta_{//} < 0$ stands for the compressive strain, and $\eta_{//} > 0$ represents the tensile strain.

III. Results and discussion

3.1 Atomic structure of FeS_2

As sketched in Fig. 1, pyrite FeS_2 adopts NaCl-like cubic structure where Fe ions are located at

face-centered cubic lattice, and S ions are arranged in dimers along <111> direction occupying the positions of Cl anions. All the Fe ions are octahedrally coordinated by six S ions at equal distances, and each S ion has three Fe neighbors and one S neighbor. The pyrite structure can be specified by two parameters, lattice constant *a* and Wyckoff parameter *u* which describes the position of S atoms. These positions are $\pm(u,u,u)$, $\pm\left(\frac{1}{2}+u,u,\frac{1}{2}-u\right)$, $\pm\left(u,\frac{1}{2}-u,\frac{1}{2}+u\right)$, $\pm\left(\frac{1}{2}-u,1/2+u,u\right)$. Our calculated lattice parameters for strain-free FeS_2 are a = 5.426 Å and u = 0.385, agreeing well with the experimental results of a = 5.418 Å, u = 0.385,[40] and the theoretical results of a = 5.422 Å, u = 0.385.[5] Our calculation shows that FeS_2 is an indirect band gap semiconductor with band gap of 0.85 eV, details about the electronic structure will be discussed in the following sections.

We firstly studied the atomic structure of FeS_2 under external biaxial and uniaxial strain ranging from -10% to 12%. The structure parameters are summarized in Fig. 2. As shown in Fig. 2(a), the in-plane lattice constants decrease with the increase of compressive strain. Meanwhile, the out-of-plane lattice constants increase slightly. Consequently, the crystal volume decreases and the bond distances of Fe-S along the *x* axis (denoted as Fe-S(⊥)) and S-S also decrease slightly as shown in Fig. 2(b) and 2(c). Previous study also reported the increase of S-S bond distance under negative pressure.[21, 22] Additional, it shows clearly in Fig. 2(c) that the Fe-S bonds along the *y* and *z* axis (denoted as Fe-S(//)) change much faster than Fe-S(⊥) and S-S bonds. Under the increasing tensile strain, the out-of-plane lattice constant decreases slightly as shown in Fig.2(a). But the crystal volume increases gradually due to the increase of in-plane lattice constant. Fe-S(//) bond length increases at the same time. We also note that the lengths of Fe-S(⊥) and S-S bond increase slightly and then decrease under the increasing tensile strain, as shown in Fig. 2(c). Moreover, all the above

mentioned structure parameters change more obviously under biaxial strain than that under uniaxial strain.

3.2 Electronic band structure of FeS_2 under strain

The above results on the atomic structure of FeS_2 revealed that S-S bond distance increases under increasing tensile strain, which also happened under the negative pressure and induce the increase of band gap.[20] Thus, we first characterized the band gap of FeS_2 subjected to tensile strain ranging from 0% to 12%. As shown in Fig. 3, there is a knee point positioned at around 6% biaxial and 10% uniaxial tensile strain. At this point, the band gap reaches to its maximum value of 1.15 eV and 1.13 eV, respectively. Similar to the phenomena indicated in Fig. 2, biaxial strain changes the band gap more evidently relative to uniaxial stain. Before the knee point, band gap increases, and then decreases after the knee point. Previous experimental and theoretical studies[20-22, 26]demonstrated that FeS_2 would turn to metal under 80 GPa positive pressure. We then investigated the electronic structure of FeS_2 subjected to compressive strains. Under the unaxial compressive strain from 0% to 10% as shown in Fig. 3, the band gap decreases gradually from 0.85 eV to 0.67 eV. It substantially decreases to 0.37 eV when FeS_2 is subjected to uniaxial strain. Therefore, it is expectable for FeS_2 to transit from semiconductor to metal under certain high unaxial compressive strain.

For comparison, we recalculated the band gap of FeS_2 under biaxial strain using the popular PBE functional. As shown in Fig. 3, the band gaps calculated by PBE functional are significantly smaller than those values computed by PBE+U. The band gap calculated by PBE+U reach its maximum under 6% tensile strain, while the PBE counterpart reach its maximum under 11% tensile strain. Note that the PBE method usually underestimates the band gap, but the Hubbard U

correction[36] gives out more accurate results. Moreover, the nonlinear behavior predicted by the two methods cannot be explained by the deformation potential theory, in which the band gap proportionally varies with the tensile strain.[41, 42] The nonlinear change of band bap under tension actually results from the shear strain component $\eta_{yz} = (\eta_{\perp} - \eta_{//})/2$. According to previous studies on the strained Si and Ge,[28, 29] shear strain splits the bottom conduction bands and change its local positions, leading to both degeneracy lifting and band warping. To test the dynamical stability of strained FeS_2, we computed the phonon spectrum of FeS_2 under 6% tensile strain. As shown in Fig.5, no imaginary phonon mode is presented, which means FeS_2 can bear 6% strain in realistic experiments.

We further studied the band structure of FeS_2 under the applied strain to gain insight into the band gap change. As we have mentioned in the above parts, uniaxial strain change the atomic structure and band gap in the similar way as the counterpart of biaxial strain, only less effectively. Thus, Fig. 4 only shows the band structures under biaxial strain of -6%, 0%, 6% and 12%. As show in Fig. 4(b) for the strain-free FeS_2, the valence band maximum (VBM) is near the X-point and the conduction band minimum (CBM) locates at Γ-point. The corresponding indirect band gap is 0.85 eV, which is close to the experimental value of 0.95 eV.[3, 25] Bandgap calculated by methods like DFT is noted as quasiparticle or fundamental bandgap, while that obtained by optical measurements include electron-hole interactions is referred as optical gap. The two values may differ substantially, the optical gap may be larger if the transition associated is indirect. Present calculated bandgap is little smaller than the experimental value, but agreeing well with previous calculation results of 0.86 eV.[8] Furthermore, we found FeS_2 is nonmagnetic at U from 0 to 4 eV, agreeing with previous studies.[5, 7-9, 43] We also found that the strained system at compressive and tensile strain from 0% to

12% are nonmagnetic. When FeS_2 is imposed with 6% biaxial compressive strain, the CBM moves down as shown in Fig. 4(a). Meanwhile, less charge transfers from Fe to S based on the Bader's charge population analysis listed in Table 1, which makes the VBM move up. Consequently, the band gap decreases from 0.85 eV to 0.62 eV. Fig. 4(c) shows the band structure of FeS_2 under 6% tensile strain, which indicates the CBM at Γ-point moves up. But, when the imposed tensile strain is larger than 6%, the CBM starts to move down and its location changes from Γ-point to R-point at 12% tension. This change results from the shear strains stated above. At the same time, more charge transfers from Fe to S as summarized in Table 1, which makes VBM moves down. CBM moves down farther than the VBM. Consequently, the band gap increase to its maximum of 1.15 eV at 6% biaxial tension and then decrease.

3.3 Optical adsorption spectra of strained FeS_2

To examine the optical absorption spectra of strained FeS_2, the absorption coefficient of FeS_2 under biaxial strain were further calculated. The calculated results at -6%, 0%, 6% and 12% strain are presented in Fig. 6. The absorption spectra of the strain-free FeS_2 starts at about 0.6 eV and the first peak locates at 2.7 eV, which agree well with the corresponding experimental observations of 0.7 eV and 2.5 eV.[44] Fig. 6 obviously shows, along both *x* axial and *y* axial, the absorption edge blue shifts with increasing the compressive strain imposed in the *yz* plane, and red shifts under the increasing tensile strain. This kind of change is not expected actually. As we have mentioned, under compressive strain, the band gap of FeS_2 decreases which normally induces red shift. On the other hand, blue shift is usually associated with increasing band gap, which is supposed to happen under 6% tensile strain. The above abnormal phenomena are not new for FeS_2. The blue shift and

decreasing band gap was observed at the same time by Batlogg *et al*[25] under positive pressure. Theoretical study[20, 22] also predicted blue shift associated with the increase of band gap under positive pressure.

Since the optical adsorption spectra of strained FeS_2 can not be explained by the band gap, we then studied the density of states (DOS) under biaxial strain of -6%, 0%, 6% and 12% as shown in Fig. 7. Fig. 6(a) shows the DOS of strain-free FeS_2. It indicates that the valence band close to the Fermi Level is predominantly composed of Fe-3d states and some S-3p states, and the conduction band near to the Fermi level is mainly constituted by S-3p states. Thus the states positioned at CBM are directly related to the S-S bond. Additional, the intensity of S-3p states is low in the conduction band below 1.35 eV, it starts to increase sharply at 1.35 eV.

The calculation results shown in Fig. 7(b) indicate, under 6% compressive strain, the S-3p low intensity states at the bottom of the conduction bond extend and the onset of sharp rise move further away from the Fermi Level relative to that of strain-free FeS_2. In the case of tensile strain, the low intensity states at the bottom of the conduction bond disappear and the sharp rises happen much closer to the Fermi Level. Based on Lazić et al.'s report,[12] the low intensity states extends the length of optical transitions in pyrite band structure, thus the onset of absorption edge is not related to the position of CBM, but is actually decided by the position where the conduction band states start to increase sharply. In this context, the blue and red shift of the adsorption edge shown in Fig. 6 are actually associated with the onset of the sharp rise in electronic-states intensity. More specifically, left move of the sharp rise in electronic-states intensity make the adsorption edge red shift, while right move of the sharp rise causes the blue shift. Most importantly, red shift of absorption edge

under the tensile strain includes the visible light adsorption spectra, that means the photon absorption of the strained FeS_2 is enhanced.

Density of states shown in Fig. 7 tell us that the states at the bottom of conduction band change from S-3p to Fe-3d when the strain is larger than 6%, which further explains the transfer of CBM from Γ-point to R-point under 12% strain. This change can be observed more clearly from the distribution of the LUMO shown in Fig. 8. In Fig. 8(a)-(c), LUMOs of FeS_2 are contributed by the S-3p states. Whereas, LUMO of FeS_2 under 12% tensile strain shown in Fig. 8(d) are comprised of Fe-3d states.

IV Conclusions

In summary, the band gap of FeS_2 increases with increasing the biaxial tensile strain to its maximum at 6% strain with enlargement of 0.30 eV. When FeS_2 is subjected to increasing compressive strain, the band gap decreases almost linearly. Uniaxial strain changes the atomic structure and band gap in the similar way as biaxial strain does, only less effective. Additional, the low intensity states at conduction band extend under the increasing compressive strain and the onset of sharp rise moves to the high energy Level, which results in the blue shift of the absorption edge. More importantly, when FeS_2 is subjected to tensile strain, the low intensity conduction states disappear and the sharp rise appears at low energy level, which makes the absorption edge red shift, and enhance the overall optical absorption. Our calculation results indicate that biaxial tensile strain can effectively improve the electronic and optical properties of FeS_2 in photovoltaic applications.

Acknowledgements

This work was supported by the National Natural Science Foundation of China (NNSFC) (Grant Nos. 21273172, 51222212, and 11102194), the program for New Century Excellent Talents in University (NCET-13-0471), the 111 Project (B08040) in China, the CAEP foundation (Grant No. 2012B0302052), the MOST of China (973 Project, Grant NO. 2011CB922200), the 111 Project (B08040).

References

1. A. Ennaoui, S. Fiechter, C. Pettenkofer, N. Alonso-Vante, K. Büker, M. Bronold, C. Höpfner and H. Tributsch, *Sol. Energy Mater. Sol. Cells*, 1993, **29**, 289-370.
2. R. Murphy and D. R. Strongin, *Surf. Sci. Rep.*, 2009, **64**, 1-45.
3. A. Ennaoui, S. Fiechter, W. Jaegermann and H. Tributsch, *J. Electrochem. Soc.*, 1986, **133**, 97-106.
4. K. Büker, N. Alonso‐Vante and H. Tributsch, *J. Appl. Phys.*, 1992, **72**, 5721-5728.
5. J. Hu, Y. Zhang, M. Law and R. Wu, *Phys. Rev. B*, 2012, **85**, 085203.
6. R. Sun, M. K. Y. Chan, S. Kang and G. Ceder, *Phys. Rev. B*, 2011, **84**, 035212.
7. L. Yu, S. Lany, R. Kykyneshi, V. Jieratum, R. Ravichandran, B. Pelatt, E. Altschul, H. A. S. Platt, J. F. Wager, D. A. Keszler and A. Zunger, *Adv. Energy Mater.*, 2011, **1**, 748-753.
8. K. Aravind, F. W. Herbert, Y. Sidney, J. V. V. Krystyn and Y. Bilge, *J. Phys.: Condens. Matter* 2013, **25**, 045004.
9. R. Sun, M. K. Y. Chan and G. Ceder, *Phys. Rev. B*, 2011, **83**, 235311.
10. Y. N. Zhang, J. Hu, M. Law and R. Q. Wu, *Phys. Rev. B*, 2012, **85**, 085314.
11. F. W. Herbert, A. Krishnamoorthy, K. J. Van Vliet and B. Yildiz, *Surf. Sci.*, 2013, **618**, 53-61.
12. P. Lazić, R. Armiento, F. W. Herbert, R. Chakraborty, R. Sun, M. K. Y. Chan, K. Hartman, T. Buonassisi, B. Yildiz and G. Ceder, *J. Phys.: Condens. Matter* 2013, **25**, 465801.
13. W. Shockley and H. J. Queisser, *J. Appl. Phys.*, 1961, **32**, 510-519.
14. S. W. Lehner, N. Newman, M. van Schilfgaarde, S. Bandyopadhyay, K. Savage and P. R. Buseck, *J. Appl. Phys.*, 2012, **111**, -.
15. J. Hu, Y. Zhang, M. Law and R. Wu, *J. Amer. Chem. Soc.*, 2012, **134**, 13216-13219.
16. R. Sun and G. Ceder, *Phys. Rev. B*, 2011, **84**, 245211.
17. B. Mao, Q. Dong, Z. Xiao, C. L. Exstrom, S. A. Darveau, T. E. Webber, B. D. Lund, H. Huang, Z. Kang and J. Huang, *J. Mater. Chem. A*, 2013, **1**, 12060-12065.
18. J. Xia, X. H. Lu, W. Gao, J. Q. Jiao, H. J. Feng and L. P. Chen, *Electrochim. Acta*, 2011, **56**, 6932-6939.
19. Q. K. Yu, S. Cai, Z. G. Jin and Z. P. Yan, *Mater. Res. Bull.*, 2013, **48**, 3601-3606.
20. V. Eyert, K. H. Höck, S. Fiechter and H. Tributsch, *Phys. Rev. B*, 1998, **57**, 6350-6359.
21. I. Opahle, K. Koepernik and H. Eschrig, *Phys. Rev. B*, 1999, **60**, 14035-14041.
22. J. Muscat, A. Hung, S. Russo and I. Yarovsky, *Phys. Rev. B*, 2002, **65**, 054107.
23. H. Zhang, X. B. Li and L. M. Liu, *J. Appl. Phys.*, 2013, **114**.
24. B. Kolb and A. M. Kolpak, *Phys. Rev. B.*, 2013, **88**, 235208.
25. A. Schlegel and P. Wachter, *J. Phys. C: Solid State Phys.*, 1976, **9**, 3363.
26. P. Cervantes, Z. Slanic, F. Bridges, E. Knittle and Q. Williams, *J. Phys. Chem. Solids*, 2002, **63**, 1927-1933.

27. H. Tahini, A. Chroneos, R. W. Grimes, U. Schwingenschlögl and A. Dimoulas, *J. Phys.: Condens. Matter* 2012, **24**, 195802.
28. Y. Sun, S. E. Thompson and T. Nishida, *J. Appl. Phys.*, 2007, **101**, -.
29. Y. M. Niquet, D. Rideau, C. Tavernier, H. Jaouen and X. Blase, *Phys. Rev. B*, 2009, **79**, 245201.
30. Y. Bi, Y. Yuan, C. L. Exstrom, S. A. Darveau and J. Huang, *Nano Lett.*, 2011, **11**, 4953-4957.
31. S. Seefeld, M. Limpinsel, Y. Liu, N. Farhi, A. Weber, Y. Zhang, N. Berry, Y. J. Kwon, C. L. Perkins, J. C. Hemminger, R. Wu and M. Law, *J. Am. Chem. Soc.* , 2013, **135**, 4412-4424.
32. G. Kresse and J. Furthmüller, *Phys. Rev. B.*, 1996, **54**, 11169-11186.
33. P. E. Blöchl, *Phys. Rev. B.*, 1994, **50**, 17953-17979.
34. G. Kresse and D. Joubert, *Phys. Rev. B.*, 1999, **59**, 1758-1775.
35. J. P. Perdew, K. Burke and M. Ernzerhof, *Phys. Rev. Lett.*, 1996, **77**, 3865-3868.
36. A. Rohrbach, J. Hafner and G. Kresse, *J. Phys.: Condens. Matter* 2003, **15**, 979.
37. H. J. Monkhorst, *Phys. Rev. B.*, 1976, **13**, 5188-5192.
38. E. Sanville, S. D. Kenny, R. Smith and G. Henkelman, *J. Comput. Chem.*, 2007, **28**, 899-908.
39. E. Aubert, S. Lebègue, M. Marsman, T. T. T. Bui, C. Jelsch, S. Dahaoui, E. Espinosa and J. G. Ángyán, *J. Phys. Chem. A*, 2011, **115**, 14484-14494.
40. N. Hamdadou, A. Khelil and J. C. Bernède, *Mater. Chem. Phys.*, 2003, **78**, 591-601.
41. J. Bardeen and W. Shockley, *Phys. Rev.* , 1950, **80**, 72-80.
42. W. Shockley and J. Bardeen, *Phys. Rev.* , 1950, **77**, 407-408.
43. S. Miyahara and T. Teranishi, *J. Appl. Phys.*, 1968, **39**, 896-897.
44. L. Vadkhiya and B. L. Ahuja, *J. Alloys Compd.*, 2011, **509**, 3042-3047.

TABLE 1: Averaged Charge Population (ρ) on Fe and Fermi level E_F under biaxial strain of -6%, 0%, 6% and 12%.

	-6%	0%	6%	12%
ρ	0.543	0.617	0.682	0.723
E_F	8.980	7.417	6.123	5.093

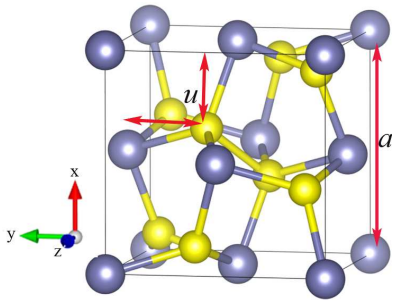

Figure 1. The unit cell of FeS_2. Violet and yellow spheres represent Fe and S atoms, respectively. *a* and *u* are the two parameters denote the lattice constant and Wyckoff parameter which describes the position of S atoms.

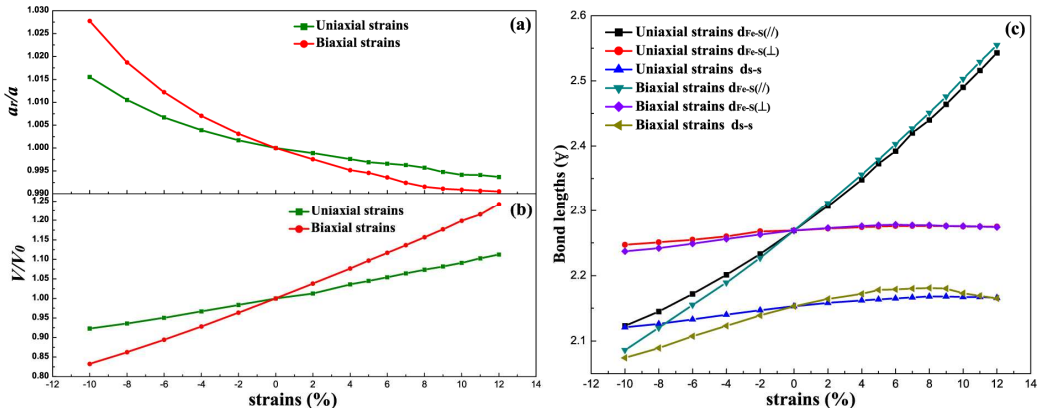

Figure 2. Calculated structure parameters of FeS_2 under biaxial and uniaxial strain. (a) Normalized out-of-plane lattice constant a_r/a, (b) normalized volume V/V_0, and (c) bond lengths of Fe-S and S-S. The bonds along the *y* and *z* axis (approximately parallel to it) are denoted as (//), and the bonds along the *x* axis (approximately perpendicular to *y*-*z* plane) are denoted as (⊥).

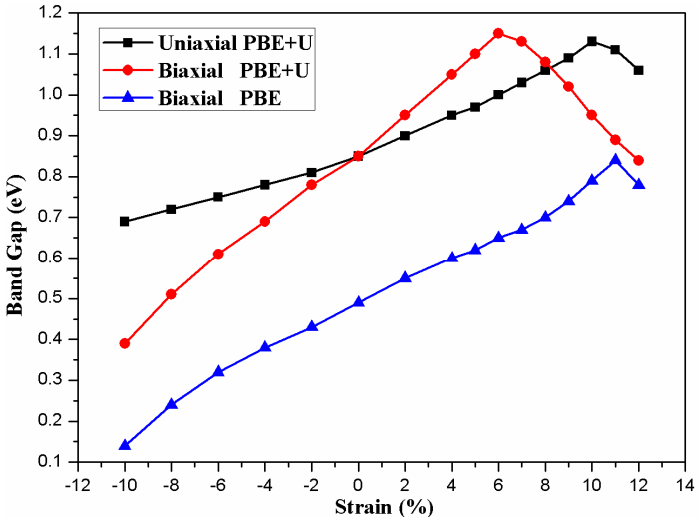

Figure 3. Calculated band gap of FeS_2 under uniaxial and biaxial strain by PBE and PBE+U functionals.

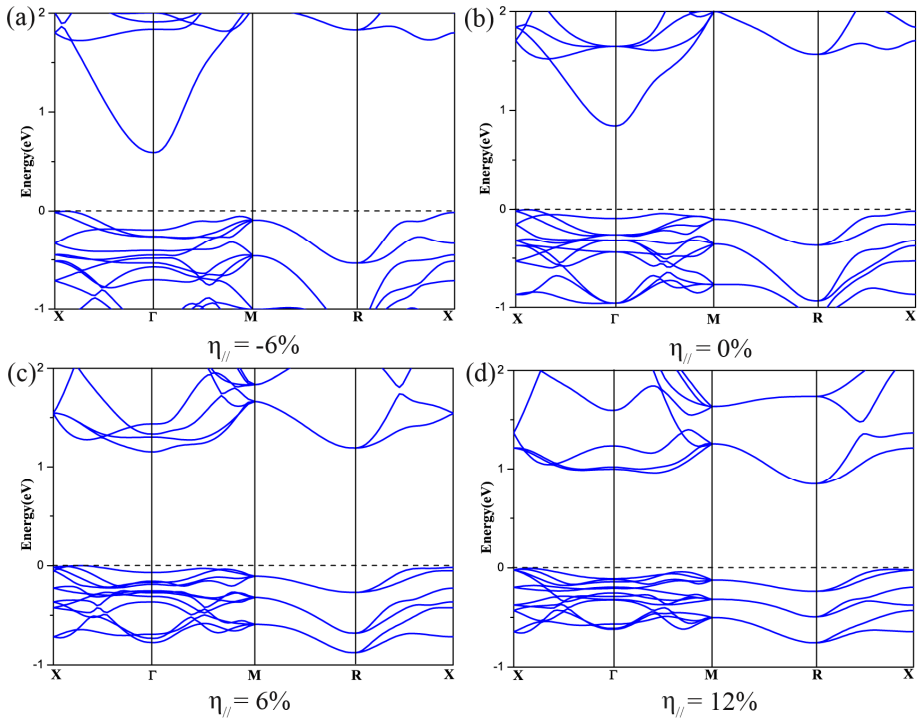

Figure 4. Band structures of FeS_2 under biaxial strain of $\eta_{//}$ = -6%, 0%, 6% and 12%. The Fermi level is set to zero.

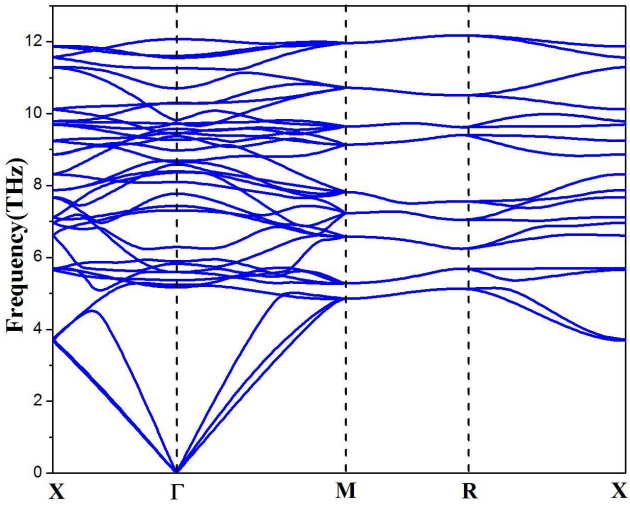

Figure 5. Phonon spectrum of FeS_2 under 6% tensile strain.

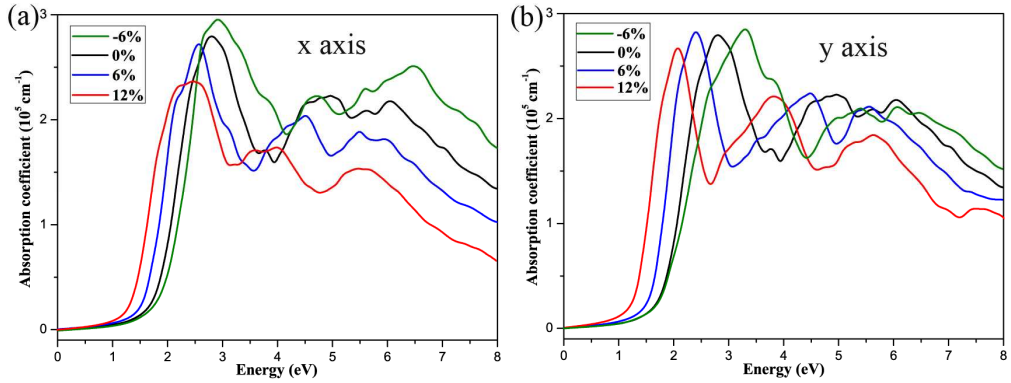

Figure 6. Absorption coefficient of FeS_2 along different direction (x axis and y axis) under biaxial strain of $\eta_{//}$ = -6%, 0%, 6% and 12%.

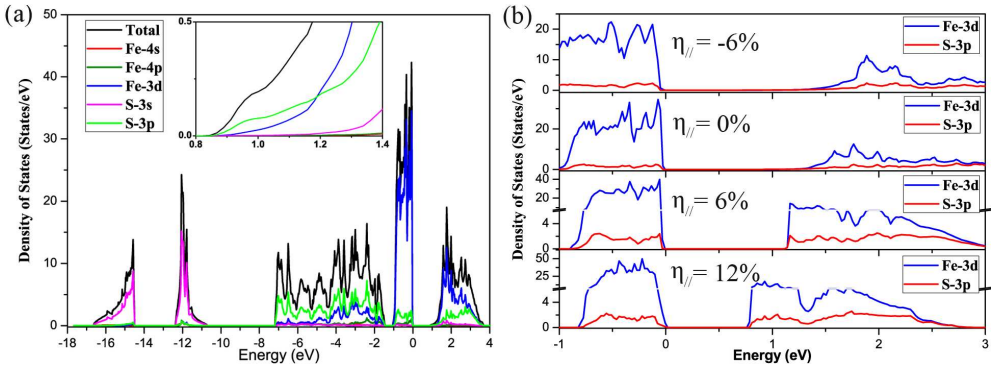

Figure 7. (a) Total and projected density of states of FeS_2. (b) Projected density of states of FeS_2 under biaxial strain of $\eta_{//}$ = -6%, 0%, 6% and 12%. The Fermi level is set to zero. The inset is a magnified view of density of states at the conduction band minimum (CBM).

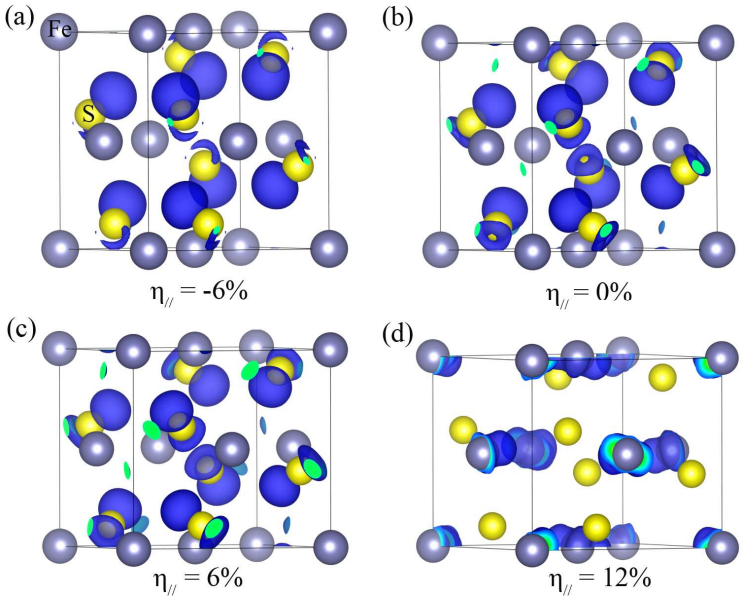

Figure 8. Contour distribution of LUMO of FeS_2 under biaxial strain of $\eta_{//}$ = -6%, 0%, 6% and 12%.

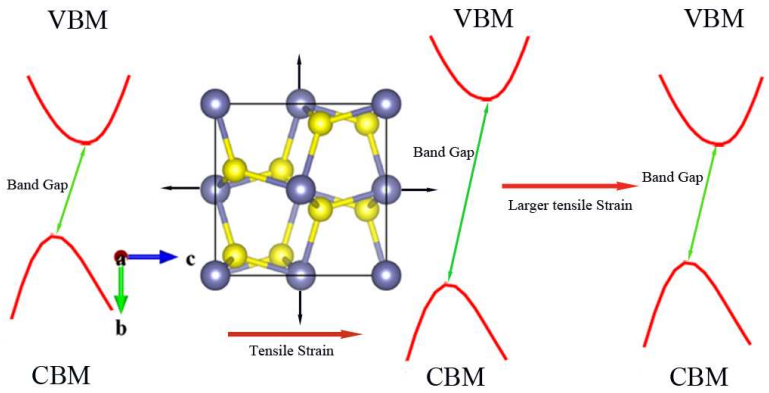

The band gap increases with increasing tensile strain to its maximum value at 6% strain, and then decreases.